Diffraction at HERA [1]

Gerhard Knies

(on behalf of the ZEUS and H1 collaborations)

Deutsches Elektronen-Synchrotron, DESY

Abstract

A survey on results from ZEUS and H1 experiments, relating to diffraction in ep collisions is presented, where the proton either stays intact or is excited into a very low mass state. The dependence of results on photon virtuality Q^2, on diffraction modes (quasi-elastic excitation of vector mesons, inelastic photon dissociation to a hadronic system X), on inclusive variables (t, W, and M_X), and on final state X topological properties is discussed in the context of hadron-hadron and parton-hadron diffraction.

[1] (presented at Les Rencontre de Physique della Vallee d'Aoste, La Thuile, March 1997

1 Introduction

Diffraction of light is a long established phenomenon. It is the elastic deflection of a light beam without a reflecting mirror, as a result of its absorption and of unitarity. At HERA, a beam of virtual photons is absorbed in ep collisions - and hence we get diffraction. The original concept of diffraction as an elastic scattering phenomenon, was extended in 1962 by Good and Walker [1] to quasi-elastic excitation of resonances with the same quantum numbers as the absorbed beam, i.e. extended to the diffraction of virtual states which the beam particles can fluctuate into. They stated: "What is virtually contained in a beam and is absorbed in the collision with a target, will be diffracted into existence." They also extended diffraction to inelastic dissociation into states with J^P changed, as diffraction of a single (virtual) subcomponent from a state which the beam particle can fluctuate into.

Hence diffraction, and at high energies equivalently the exchange of a pomeron, can be used to inspect the virtual hadronic and partonic content of the virtual photon beam coming in via a fluctuation of the beam electrons as $e \to e' + \gamma$ and the further fluctuation $\gamma \to$ vector mesons, $q\bar{q}$, $q\bar{q}g, ..$ [2, 3, 4], in the process $e + p \to e' + X + Y$ (see Fig. 1) with a large rapidity gap between the hadron systems X and Y.

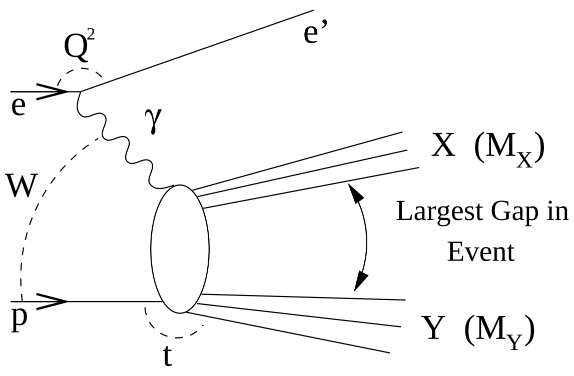

Figure 1: Illustration of the process, $ep \to e'XY$, in which the hadron systems X and Y are separated by the largest rapidity gap in the event. W is the invariant mass of the colliding virtual photon - beam proton system. $-Q^2$ is the 4-momentum transfer at the (e, e') and t at the (p, Y) vertex. M_X and M_Y are the masses of systems X and Y, respectively.

In these events the beam proton either stays intact (Y = proton in Fig. 1) or is excited to a low mass baryonic system Y, by a colourless exchange with a small transverse component in the momentum transfer [2] $I\!P = p - Y$. In a diffractive process the 4-momentum transfer $t = (\gamma^* - X)^2 = (p - Y)^2$ is small and the invariant masses M_X^2, M_Y^2 are much smaller than $s = (e + p)^2$. The incoming photon, ranging from very low to high virtuality, can be excited into a vector meson, or dissociate into a high mass state X

diffractive excitation	$\gamma^{(*)} \to X$= vector meson or
diffractive dissociation	$\gamma^{(*)} \to X \neq$ vector meson.

Large-Rapidity-Gap (LRG) events at the ep collider HERA have been observed in the ZEUS [5] and in the H1 [6] experiments. They are, not exclusively but mainly, attributed to diffraction. Events with no activity over a large pseudo-rapidity range adjacent to the outgoing proton beam (forward direction), or with a track measured in the leading proton spectrometer (Zeus) with a momentum near proton beam energy are selected.

In the photon fluctuation view, utilized above, the hadronic as well as the partonic content of real or spacelike photons is made visible by a mainly soft diffraction process of partons off the proton, for which the amplitude in detail is unknown.. The special case of diffractive dissociation of highly virtual photons can also be interpreted as the electron probing the partonic content of the pomeron [7, 8]. In this view an yet unknown pomeron structure function together with an unknown pomeron flux of the proton, is introduced [9]. These two views are supposed to be equivalent - where applicable - and they may be used to supplement each other by exploiting different kinds of physics knowledge for understanding diffraction.

The virtual hadronic and partonic content of timelike photons has been studied in e^+e^- annihilation experiments. The couplings of photons to quarks and to the vector mesons $\rho, \omega, \phi, J/\psi$ and Υ are well known. The high collision energy of the ep beams at HERA, the large range in Q^2 of the photons, and the fact that the photons have only a few GeV of energy in the laboratory system make HERA an ideal place to measure and study diffractive excitation and dissociation of photons. Hence the LRG events from HERA can contribute to the understanding of the diffractive interaction of the partonic configurations of photons, i.e. of the diffraction of partons off protons.

In this talk [3] a brief survey will be given on results for vector meson production and

[2] Here, and throughout this paper the term pomeron and the symbol $I\!P$, are used for the exchanged object independently of its nature, when the difference between a pomeron and a subleading reggeon exchange does not matter.

[3] The experimental results shown represent mainly the status of analyses presented at the XXVIII Int. Conf. on High Energy Physics, Warsaw, Poland, July 1996 [10]. The results are selected in accordance with the ZEUS and H1 collaborations. The presentation is under the responsibility of the author.

for dissociation.

2 A brief reminder of hadron-hadron diffraction

The total and the diffractive elastic cross sections for hadron-hadron collisions, are known to be dominated by soft processes. Hard processes in hadron-hadron scattering are connected with the generation of particles with large p_t, i.e. with $p_t > 1/R_p$. They are ascribed to the collision of partons from the colliding hadrons. Hard diffraction of hadrons requires that their partonic content is resolved in the diffraction processs.

The energy dependence of σ_{tot} has been parameterized (see Fig. 2) as

$$\sigma_{tot}(W) = \sigma_{\mathbb{P}} * (W/W_0)^{2\epsilon} + \sigma_R * (W/W_0)^{2\eta} \tag{1}$$

with a reggeon exchange term (σ_R) and a pomeron term ($\sigma_{\mathbb{P}}$). The value of the exponent of the pomeron term, i.e. $\epsilon = 0.08$ is taken as signature for soft processes. For hard processes larger values are expected. The total cross section of almost real photon proton scattering shows the same *soft* energy dependence. This can be seen from Fig. 2.

The optical theorem relates elastic diffraction to the total cross section:

$$\frac{d\sigma^{diff}}{d|t|}|_{t=0} = \frac{\sigma_{tot}^2}{16\pi} \propto (W/W_0)^{4\epsilon}$$

The pomeron Regge trajectory $\alpha_{\mathbb{P}}(t)$ is related to ϵ: $\alpha_{\mathbb{P}}(t) = \alpha_{\mathbb{P}}(0) + \alpha'_{\mathbb{P}} * t$, with $\alpha_{\mathbb{P}}(0) - 1 = \epsilon = \lambda$ where λ and ϵ are symbols used equivalently in the literature. Correspondingly, when the energy dependence of a diffractive process like quasi-elastic vector meson production is steeper than for elastic hadron hadron scattering, it is attributed to diffraction at a subhadronic scale, to hard diffraction, respectively.

3 Results on Total Cross Section for Virtual Photons

The energy dependence of $\sigma(\gamma p)$ changes with Q^2 when the photon gets virtual. This can be seen from Fig. 3 which shows $\sigma(\gamma p)$ and $\sigma(\gamma^* p)$ for Q^2 up to 3000 GeV^2. The energy dependence is getting steeper with growing photon virtuality, corresponding to $\epsilon > 0.08$ for $Q^2 \gtrsim 1$ GeV^2. This deviation from the soft energy dependence is ascribed to the growing importance of hard or short distance processes, for photons getting more and more virtual.

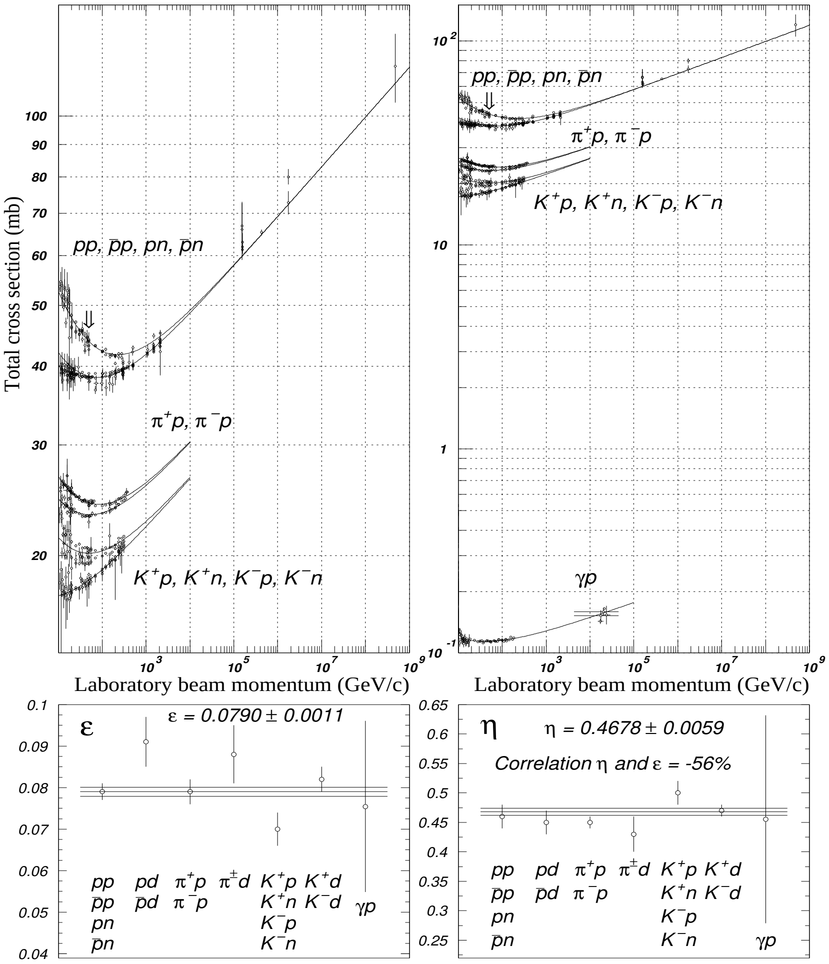

Figure 2: Total Hadronic and γp cross sections(top), and fit results to exponents for cross sections. (PDG, Phys. Rev. D54 (1996) 192)

4 Results on Vector Meson Production

At the large energies of HERA the reggeon contribution can be neglected and the cross section for quasi-elastic vector meson production has the momentum transfer (t) and energy (W) dependence

$$\frac{d\sigma(W,t)}{dt} = \frac{d\sigma(W_0, t=0)}{dt} * (W/W_0)^{4\epsilon} * e^{bt} \quad (2)$$

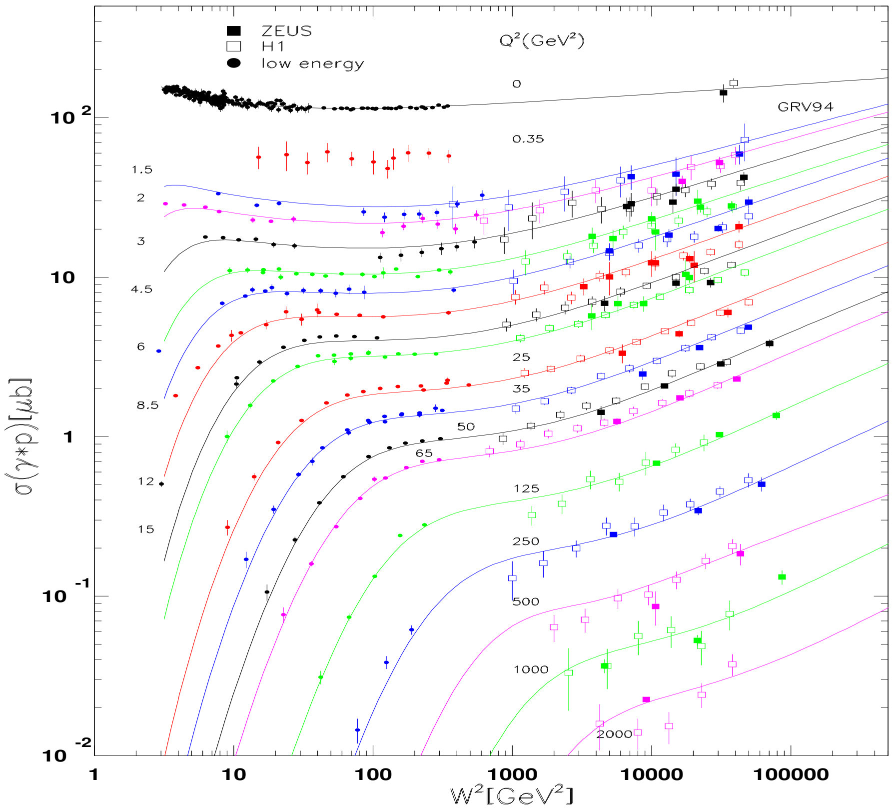

Figure 3: Energy dependence of $\sigma(\gamma^* p)$ in Q^2 bins for 1994 data, and NLO fit.

with a shrinkage in the diffractive slope

$$b(W) = b_0 + 4\alpha'_{I\!P} \cdot \ln(W/W_0) \tag{3}$$

4.1 W dependence

Because of the shrinkage of the diffraction peak with W the t-integrated elastic cross section has a W dependence W^δ with $\delta < 4 \cdot \epsilon$. Fig. 4 shows the energy dependence of the total elastic cross section for photoproduction of various vector mesons. It shows the same soft dependence for the light vector mesons ρ, ω and ϕ, but a much steeper one for J/ψ production. This is interpreted [11] as being due to the fact that the large charm quark masses make the J/ψ meson smaller than required by confinement, and hence make J/ψ photoproduction a short distance or a hard process, respectively. A perturbative treatment as a 2-gluon exchange process with the gluon density $g(\bar{x})$ of the

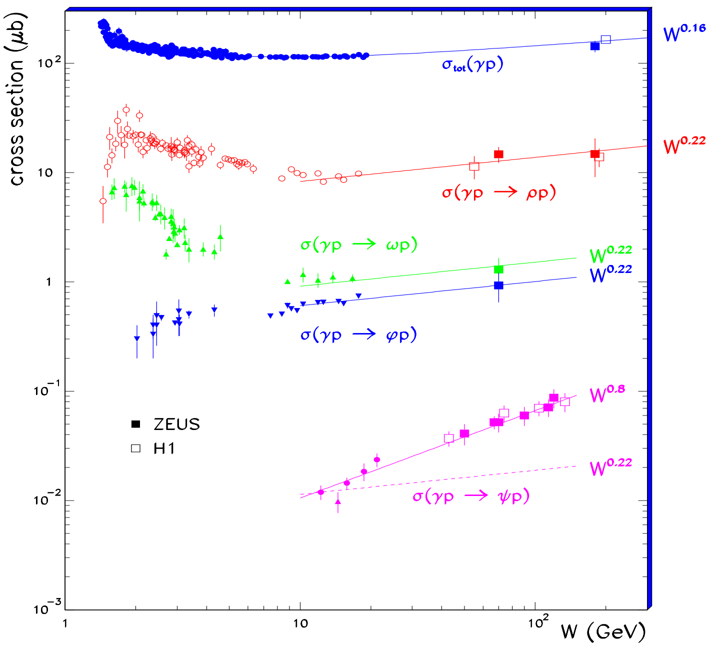

Figure 4: Energy dependence of photoproduction cross section for vector mesons.

proton, yields a cross section $\sigma \propto |\bar{x}g(\bar{x}, \bar{Q}^2|$ with $\bar{x} = (M_\psi/W)^2, \bar{Q}^2 = (M_\psi/2)^2$, which shows a W dependence steeper than the soft one and is compatible with the data.

The same modification of the W dependence occurs when the incoming photon takes a spacelike mass Q^2 far away from the light vector meson masses. Figure 5 shows the W dependence for Q^2 values from 3.7 to 20 GeV^2. Here, data from HERA at $W \sim 100$ GeV and from fixed target experiments at $W = 13$ GeV are combined. A value of $\delta = 0.55$ gives a proper description of the W dependence at $Q^2 = 20\text{GeV}^2$, while $\delta = 0.22$ as in photoproduction is not acceptable.

If both, the incoming photon and the outgoing vector meson have (mass)^2 values far away from the light vector mesons, the energy dependence does not get more steep than in the single large (mass)^2 case, as shown in Fig. 6. In other words, as soon as at least one (mass)^2 involved in $\gamma \to VM$ is absolutely larger than order(1 GeV^2), the quasi-elastic vector meson production cross section shows a W dependence clearly steeper than observed for soft processes and agrees with the expectations for the W dependence derived from the gluon density inside protons [11].

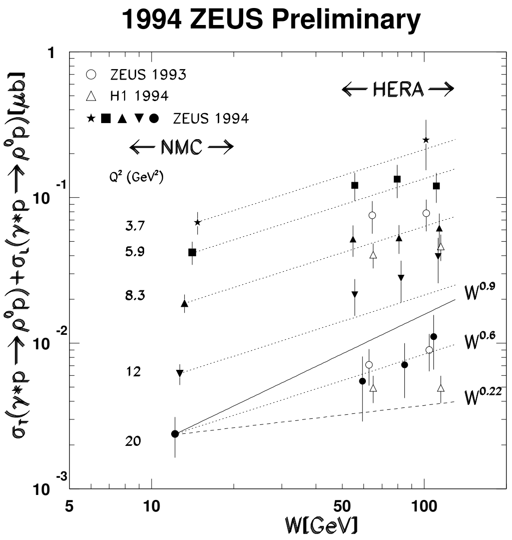

Figure 5: Energy dependece of quasi-elastic ρ meson production by virtual photons of growing virtuality.

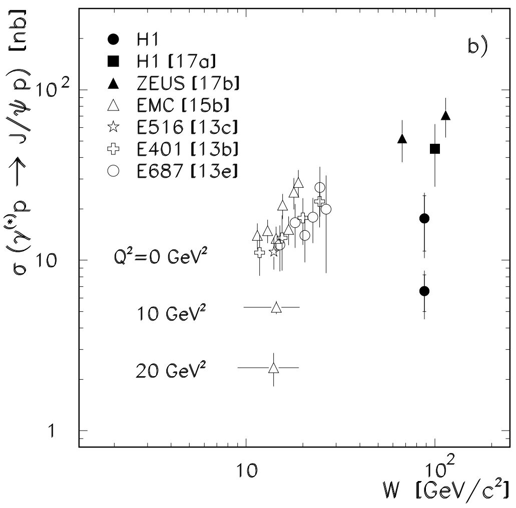

Figure 6: Energy dependece of quasi-elastic J/Ψ meson production by photons of growing virtuality.

4.2 t dependence

The slope b of the diffraction peak (see eq.2) is in the optical model connected with the transverse size (radius R) of the respective absorption cross section by $b = R^2/5$ for a

Gaussian density of the absorbers. For a number of reactions b has been measured. In Fig. 7 we show the ZEUS measurement of this slope in elastic ρ photoproduction, with the ZEUS forward proton spectrometer. The slope found here is $b = 9.6 \pm 0.8 \pm 1.1\ \mathrm{GeV}^{-2}$. Results for further reactions are given in Table 1. With the present statistics of the HERA

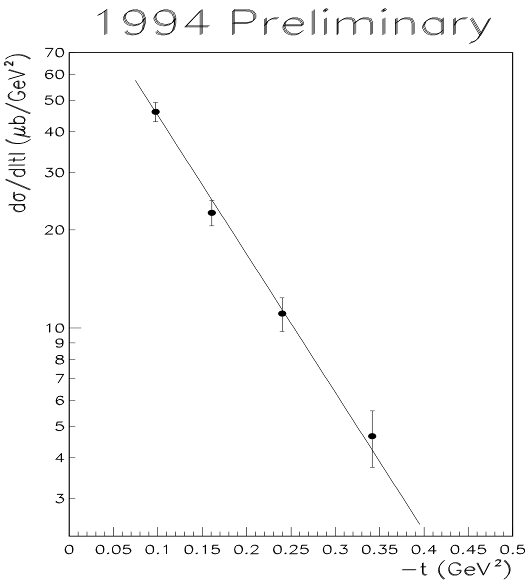

Figure 7: t dependence of the differential cross section for ρ photoproduction at $\langle W \rangle = 70$ GeV and $Q^2 < 4\ \mathrm{GeV}^2$, measured with the ZEUS leading proton spectrometer.

data there is no significant evidence yet for a shrinkage of the diffraction peak - with a size of $\alpha'_{I\!P} = 0.25$ in eq.(3) - for virtual photons.

4.3 Hadronic versus partonic diffraction

Table 1 gives a survey on average b and δ values from diffractive processes classified by their number of vertices with *coherence at the hadron scale* R_p (N_{CHS}). Coherence at the hadron scale is defined by the longitudinal momentum transfer Δp_l to be $\lesssim 1/R_p$, in the rest frames of the emerging systems X and Y, respectively, required to induce the transitions $\gamma + I\!P \rightarrow X$ and $p + I\!P \rightarrow Y$.

Reaction (at $W_{\gamma p} \simeq 90$ GeV)	b/GeV^2 e^{bt}	δ W^δ	No of vertices with coherence at hadron scale
$\gamma p \ \rightarrow \rho \ p$	10 ± 1	0.22	2
$\gamma p \ \rightarrow \rho \ p$	6 ± 1.5	0.6	1
$\gamma \ p \rightarrow J/\psi \ p$	4 ± 0.5	0.8	1
$\gamma^* \ p \rightarrow J/\psi \ p$	4 ± 2	0.6	1
$\gamma \ p \rightarrow \rho \ p_{disso}$	5.3 ± 0.7		1
$\gamma^* \ p \rightarrow X \ p$	5.9 ± 1.6		1
$\gamma^* \ p \rightarrow \rho \ p_{disso}$	$2. \pm 0.5$		0
$\gamma \ p \rightarrow J/\psi \ p_{disso}$	1.6 ± 0.5		0

Table 1: W and t dependence of diffractive dissociation reactions, ordered by the number of vertices with coherence at hadron scale (N_{CHS}). The errors on b are estimates, to include the difference between different measurements.

4.4 Q^2 dependence

The "Q^2 - knob" for tuning the virtual photon through a large Q^2 range is the very special feature of the HERA experiments. Firstly the ratio of longitudinal to transverse helicity components in the photon changes with Q^2. This is visible in the helicity angle distribution of vector meson decays, shown in Fig. 8 for the $\rho \rightarrow \pi^+\pi^-$ decay. The transition $\sigma_L > \sigma_T$ occurs near $Q^2 = 1$ GeV^2. From ZEUS and H1 data on $\rho \rightarrow \pi^+\pi^-$ and $\phi \rightarrow K^+ \ K^-$ the following $R = \sigma_L/\sigma_T$ values are found: $Q^2 \simeq 0: \ R < 0.04$; $Q^2 = 0.34: \ R = 0.26 \pm 0.04$; $Q^2 = 0.61: \ R = 0.56 \pm 0.09$, $(6 < Q^2 < 20): \ R = 3.3 \ +4 - 1.4$. Secondly, the photon coupling to the various vector mesons relative to $q\bar{q}$ non resonant Fock states depends on Q^2, in contrast to the electromagnetic coupling to $q\bar{q}$. Also the quasi-elastic diffraction amplitudes for virtual vector mesons may depend on Q^2. The amount of diffraction into such states is therefore of interest. Fig. 9 shows the ratio $\sigma_{el}(\gamma^* \rightarrow VM)/\sigma_{tot}(\gamma^* p)$ for $VM = \rho, J/\psi$, and $\sigma_{diss}(\gamma^* \rightarrow X)/\sigma_{tot}(\gamma^* p)$ as a function of Q^2. This figure shows very clearly, that the fraction of diffraction dissociation is almost independent of Q^2, with about 15% of σ_{tot}, for $Q^2 = 0$, and with about 10% for $Q^2 = 10, \ 20$ GeV^2, while the fraction for ρ declines by a factor of 100 over the same range. We observe here the transition from *vector meson dominance* to *vector meson insignificance*, or the disapearance of the *hadronic* in comparison with the *pointlike* photon as a function of Q^2. The diffractive fraction of J/ψ is - within large errors - not reduced by growing Q^2, similar as that for diffraction dissociation. At $Q^2 = 20$ GeV^2 the diffractive

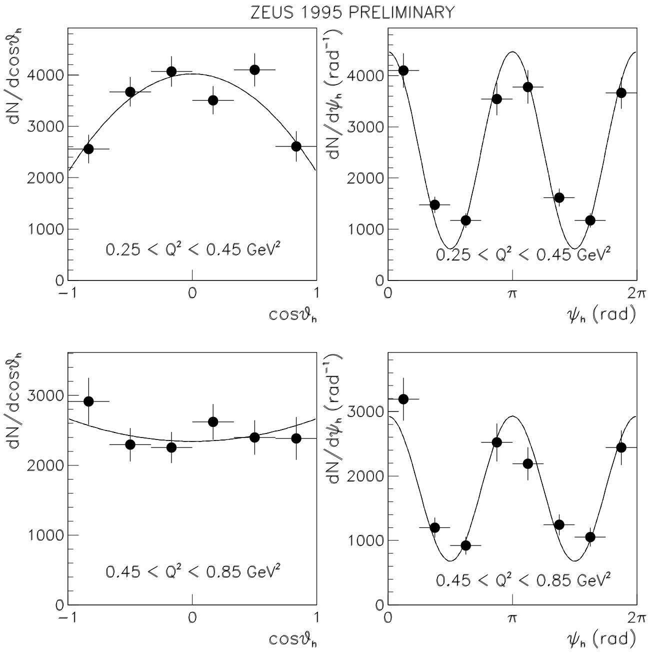

Figure 8: Acceptance corrected helicity angle distributions from ρ decays from quasi-elastic production

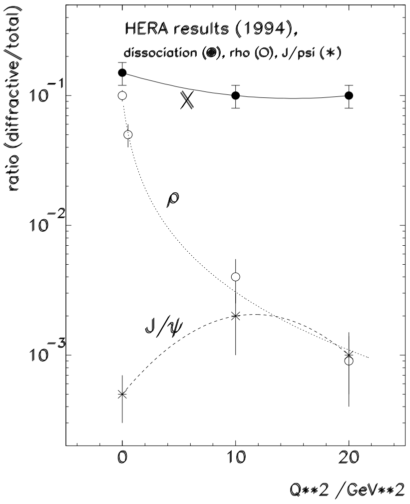

Figure 9:Ratio of diffractive to total cross section for photon dissociation (X), excitation to ρ, and to J/ψ as a function of Q^2. The values are estimated averages from ZEUS and from H1 data. Also the errors are estimates, to give the order of magnitude of accuracy. The average energy for these data is $W_{\gamma\ p} = 90$ GeV. The curves are to guide the eye.

fraction of the ρ is no longer enhanced over the J$/\psi$. The Q^2 dependence of the various fractions is consistent with a picture in which the contribution to diffraction from the partonic components of the photon, i.e. of its fluctuation into non-resonant $q\bar{q}$, are 10%, independent of Q^2, while contributions from its hadronic components - dominated by the ρ - are visible at $Q^2 = 0$ in terms of the quasi-elastic ρ production and in terms of a contribution with nearly comparable size from diffractive dissociation of the hadronic ('resolved') photon.

5 What the continuum can tell us

When the final state X is not a vector meson resonance, diffractive dissociation of photons can be seen as a fluctuation of the the photon into a parton configuration with one virtual parton, which is then diffracted off the proton 'into existence' [1, 2, 3, 4], whereby it receives a longitudinal momentum transfer Δp_l which in the outgoing proton rest frame is small, but in the X frame large ($\simeq M_X/2$). Photons have two sources for partons: from their hadronic vector meson states and from their direct coupling to $q\bar{q}$ pairs. As Fig. 9 showed, at $Q^2 > 10$ GeV^2 the direct coupling dominates. The processes of virtual photons leading to 2- and 3-parton configurations are sketched in the diagrams of Fig. 10. These diagrams can also be read as DIS off a pomeron with a partonic content [9, 7, 8]. The simplest partonic dissociation process (Fig. 10a) was discussed first by Bjorken and Kogut [12], in terms of the Aligned Jet Model (AJM). Here, configurations with large parton momenta k_t transverse to the collision axis have a reduced cross section in comparison with the expectation for the collision of single partons with the proton. This suppression of large k_t has been explained in terms of "colour transparency" [13], since the transverse separation of the $q\bar{q}$ state is then small on average, leading to a small colour dipole moment, or to mutual screening, respectively. However, $q\bar{q}$ configurations with a small transverse momentum difference have a large transverse separation. They do not develop such screening and hence are not suppressed by their interaction with the proton. In the rest frame of X, the AJM picture thus leads to a back-to-back 2-jet configuration with small jet transverse momenta P_t relative to the incoming proton beam direction, typical of soft interactions.

The necessity to incorporate into this model gluons radiated by the $q\bar{q}$ system was already pointed out in [14]. Extensions along these lines have been studied further by several authors [2, 3]. This QCD extension is related in the DIS-off-pomerons picture to a QCD evolution of the structure function of the diffractive exchange. In this picture the description of diffractive dissociation is furnished by parton densitiy distributions in the pomeron. Because of the connection of pomeron exchange to a total cross section, there

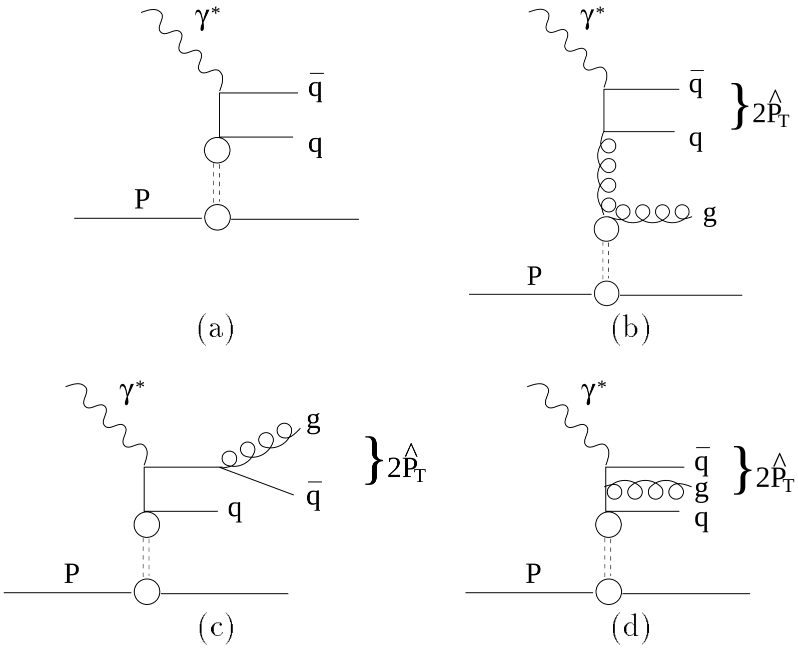

Figure 10: Diagrams for LRG events: Born term diagram (a), boson-gluon fusion (BGF) (b), QCD-Compton (QCD-C) (c, d). The $q \leftrightarrow \bar{q}$ exchanged configurations are implied.

are constraints on the parton densities in the pomeron. Since the colour charge of gluons is larger than of quarks we expect $\sigma(gluon, proton) > \sigma(quark, proton)$. A ratio of $\mathcal{O}(10)$ is estimated in [4]. This implies the gluon density in the pomeron must be larger than the quark density. The involvement of partons in the diffraction processes (see Fig. 10) will coin the M_X and Q^2 dependence of the inclusive cross section for LRG events, and the topology of the final state X.

5.1 Inclusive cross section for diffractive dissociation

The inclusive cross sections have been analysed by H1 and ZEUS in terms of a diffractive structure function $F_2^{D(3)}$ as defined in Fig. 11. Fig. 11 shows the H1 measurement at two β points at $Q^2 = 20$ GeV^2. The full β and Q^2 range for the H1 measurement is visible from Fig. 12. The H1 analysis performs a separation of contributions from pomeron and from reggeon exchange. Figure 11 summarizes the results of H1. Zeus has measured this structure function with LPS data, requiring a measured track with

? Hard Diffraction in DIS ?

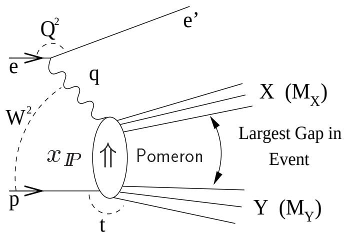

$$x_{I\!P/p} = x_{I\!P} \approx \frac{Q^2+M_X^2}{Q^2+W^2}$$

$$x_{q/I\!P} = \beta = \frac{x}{x_{I\!P}} \approx \frac{Q^2}{Q^2+M_X^2}$$

$$\frac{d^3\sigma^D_{ep\to e'XY}}{d\beta \; dQ^2 \; dx_{I\!P}} = \frac{4\pi\alpha^2}{\beta Q^4}\left(1-y+\frac{y^2}{2}\right) F_2^{D(3)}(\beta, Q^2, x_{I\!P})$$

94 Data $\longrightarrow$ Analysis of n_1, n_2 in :

$$F_2^{D(3)} = F_2^{I\!P}(\beta, Q^2)\cdot x_{I\!P}^{-n_1} + C_M \cdot F_2^M(\beta, Q^2)\cdot x_{I\!P}^{-n_2}$$

For $F_2^M = F_2^\pi$(GRV), $x_{I\!P} < 0.05$, and $M_Y^2 < 1.6$ GeV^2:
$+$ interference with phase angle of 45°

H1 Preliminary 1994

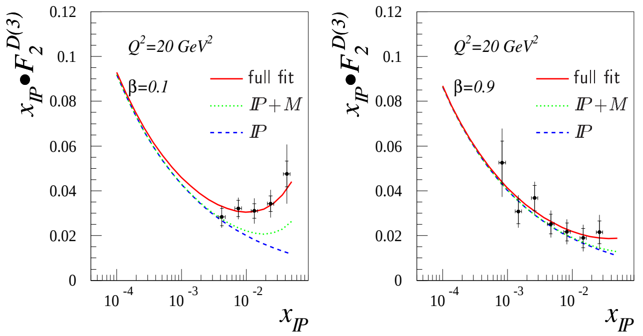

$$n_1 = 1.29 \pm 0.03 \quad n_2 = 0.3 \pm 0.03 \quad n \simeq 2\alpha(0) - 1 \Longrightarrow$$

$$\alpha_{I\!P}(0) = 1.18 \pm 0.02 \pm 0.04$$

Figure 11: Information and results on the $F_2^{D(3)}$ analysis by H1.

momentum $p > 0.97\ p_{beam}$, at $\langle Q^2\rangle = 12\mathrm{GeV}^2$. This is shown in Fig. 13. The $x_{I\!P}$ range used in the ZEUS analysis is lower than in the H1 experiment. No reggeon separation is therefore performed. In the notation of Fig. 11 the results are

$$\text{ZEUS} \quad n_1 = 1.28 \pm 0.07 \pm 0.15 \quad \alpha_{I\!P}(0) = 1.18 \pm 0.04 \pm 0.08$$

$$\text{H1} \quad n_1 = 1.29 \pm 0.03 \quad \alpha_{I\!P}(0) = 1.18 \pm 0.02 \pm 0.04$$

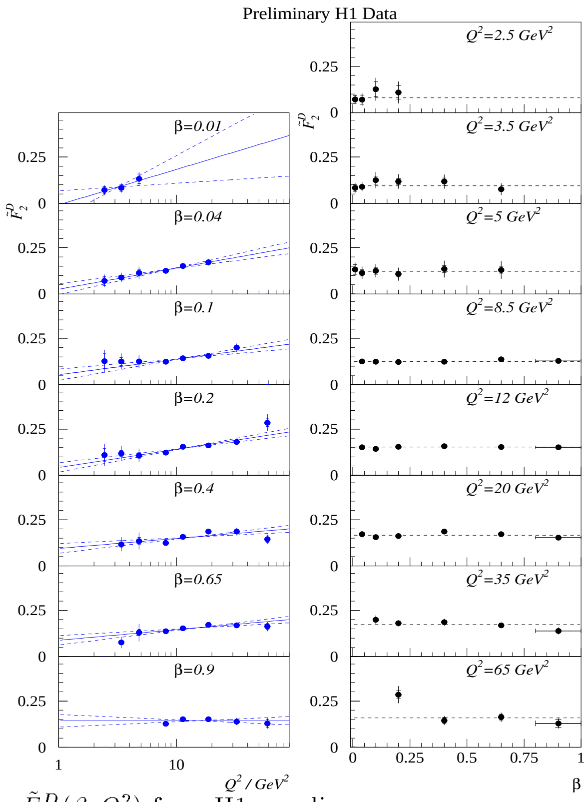

Figure 12: Results on $\tilde{F}_2^D(\beta, Q^2)$ from H1 anaylis.

H1 has in addition performed a QCD analysis by exploiting the $F_2^{D(3)}$ measurements in a fit of boundary conditions for quark and gluon density distributions at a starting scale using a perturbative DGLAP QCD evolution. As starting scale the value $Q_0^2 = 3\mathrm{GeV}^2$ was chosen. The result of this fit is that $80-90\%$ of the pomeron momentum is carried by gluons. This confirms the expectation for a gluon dominance of the diffractive exchange.

Figure 12 also shows the integral over $x_{\mathbb{P}}$ from 0.0003 to 0.05 of $F_2^{D(3)}(\beta, Q^2, x_{\mathbb{P}})$, at sets of β, Q^2 points. $\tilde{F}_2^D(\beta, Q^2)$ shows clear scaling violations in terms of a Q^2 dependence. It is compatible with independence on β, and different from a hadron (pion) like behaviour as proportional to (1-β) for $\beta > 0.5$.

5.2 Topological properties in final states

The involvement of gluons is always connected with (at least) 3-parton configurations, while diffraction processes with quarks can also lead to 2-parton configurations (Fig. 10). In e^+e^- annihilation the event shape variable thrust (T) [15, 16] was quite instrumental

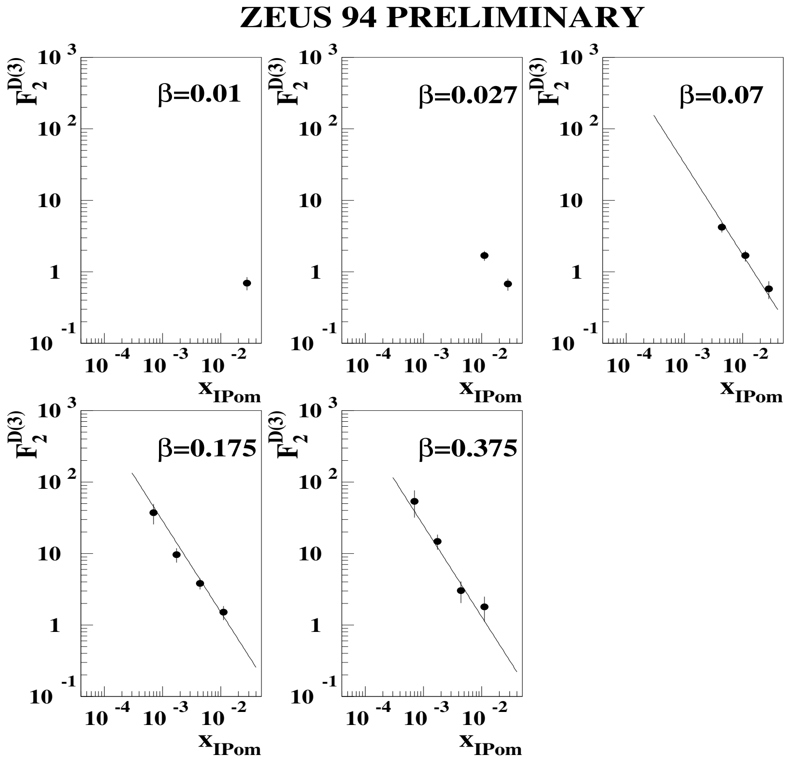

Figure 13: $F_2^{D(3)}$ measurement by ZEUS, using tagged protons.

to measure the ratio of $q\bar{q}$ to $q\bar{q}g$ configurations even at energies $\sqrt{s_{ee}}$ too low to resolve 3-jet from 2-jet events [17], without jet algorithms. In the centre of mass of a system X of N particles, the thrust method determines the direction of the unit vector $\vec{a}$ along which the projected momentum flow is maximal [15], and $1 - T$ measures the deviation of the momentum flow from colinearity ($T = 1$). Thrust is computed as [16]:

$$T = (1/\sum_{i=1}^{N} |\vec{p}_i|) \cdot \max_{\vec{a}} \sum_{i=1}^{N} |\vec{p}_i \cdot \vec{a}|$$

where $\vec{p}_i$ represents the momentum of particle i, in the rest frame of the N particles. The N paricles can then be separated into two subsets with $\vec{p}_i \cdot \vec{a} < 0$ and > 0, respectively, i.e. into 2 *thrust jets* with jet momenta as the sum of the momenta of the respective particles. In case of a genuine 3-jet event, the thrust value is reduced, and the thrust direction follows the direction of the largest momentum jet - in the respective overall restframe.

Because of the forward rapidity gap requirement, the hadronic final states of the accepted events are well contained in the central detectors of the HERA experiments, providing measurement conditions similar to those in e^+e^- annihilation at symmetric

e^+e^- colliders. Since no jet energy threshold is required in the thrust method, all events in the M_X range under study can be included.

Fig. 14a shows the H1 measurement of the average thrust, for $10 < Q^2 < 100$ GeV^2, $M_Y < 1.6$ GeV and $x_{\mathbb{P}} < 0.05$, corrected for acceptance and for detector resolution, as a function of $1/M_X$, in seven M_X intervals in the range 4 to 36 GeV.

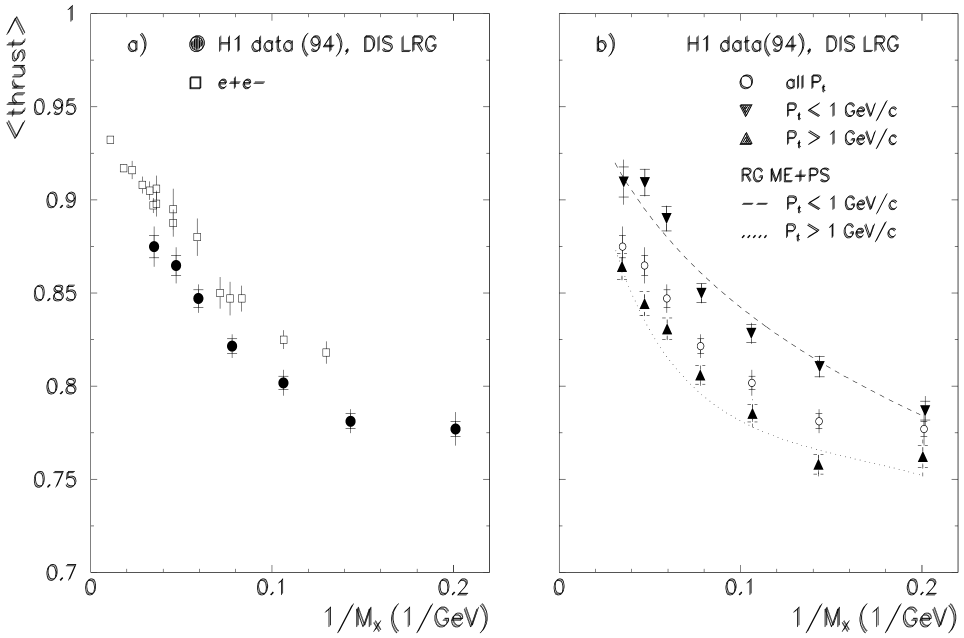

Figure 14a: Average thrust $\langle T \rangle$, as a function of $1/M_X$, for LRG data and for e^+e^- annihilation data.

Figure 14b: Average thrust $\langle T \rangle$, as a function of $1/M_X$, for all events, for events with $P_t < 1$ and for events with $P_t > 1$ GeV/c. The curves are from a MC simulation described in the text.

The correlation of thrust with $1/M_X$ rather than M_X is shown because it allows in a transparent way to distinguish between perturbative and hadronization effects on thrust. For $M_X \to \infty$ the latter should become negligible.

Fig. 14a includes for comparison the available data for thrust in e^+e^- annihilation [17, 18] plotted at $M_X = \sqrt{s_{ee}}$. In e^+e^- annihilation, data on the evolution of thrust with $\sqrt{s_{ee}}$ allowed a separation of hadronization from perturbative QCD effects. In LRG events the partonic structure and hadronization effects may be different from those in e^+e^- annihilation. The correlation of thrust with M_X may be exploited here as well to separate those two contributions. We note the following gross features:

1. $\langle T \rangle$ increases with M_X. Since the particle multiplicity also increases with M_X, this implies that the final state is not isotropic, because then $\langle T \rangle$ would fall, and approach 0.5 when $1/M_X \to 0$. The growth of $\langle T \rangle$ is the signature for a growing back-to-back correlation of the momentum flow when the final state mass increases. Hence, the thrust direction corresponds to an effective topological axis of the event.

2. There is a striking similarity between the $\langle T \rangle$ dependences in e^+e^- annihilation and virtual photon dissociation, under the assumption that the role of $\sqrt{s_{ee}}$ in e^+e^- annihilation is played by M_X in the DIS LRG events. The M_X dependence appears to be the same, and $\langle T \rangle$ of DIS LRG events is lower by an approximately constant value of $0.025 \pm 0.004 \pm 0.006$.

The result $\langle T \rangle_{LRG} < \langle T \rangle_{ee}$ implies that the final state in DIS LRG events cannot be understood as a simple $q\bar{q}$ state with standard limited p_t hadronization [19], and it requires that higher parton multiplicities are even more important than in e^+e^- annihilation. A quantitative interpretation of the difference $\langle T \rangle_{LRG} - \langle T \rangle_{ee}$ in terms of contributions from Born-term, QCD-Compton and BGF subprocesses (see Fig. 10) requires an integration over the different non-perturbative diffractive processes, or over the parton densities of the diffractive exchange, respectively. These are not available at present.

The presence of underlying configurations with three - as in the diagrams in Fig. 10b, c and d - or more partons can also be studied with the correlation between P_t, the thrust jet momentum relative to the γ^* p collision axis, and thrust. In hadron final states emerging from $q\bar{q}$ configurations, P_t can come from non-aligned, i.e. tilted $q\bar{q}$ states. T is then independend of P_t. Fig. 14b shows that $\langle T \rangle$ is strongly correlated with P_t at each M_X point. This correlation demonstrates on purely kinematic grounds the presence of configurations with at least 3 non-colinear partons. Studies with simulated events confirm that the difference in $\langle T \rangle$ between the two P_t-samples is compatible with coming from configurations with two and three partons. This is seen in the curves in Fig. 14b, which present the expectations for $q\bar{q}$ and $q\bar{q}g$ configurations, as generated by the MC program RAPGAP [20] in the matrix element mode for the boson-gluon fusion and QCD-Compton processes shown in Fig. 10.

The result $\langle T \rangle_{LRG} < \langle T \rangle_{ee}$ is also observed in the ZEUS experiment. The data in Fig. 15 are selected with a pseudorapidity cut of $\eta_{max} < 1.8$ in comparison with $\eta_{max} < 3.2$ in the H1 data. This implies larger acceptance loss effects in the ZEUS data. They are not corrected for the $\eta_{max} < 1.8$ cut.

In addition, the alignment, i.e. the correlation of the thrust direction with the $\gamma^* p$ direction in the X rest frame, can be studied in terms of the P_t distribution of thrust jets

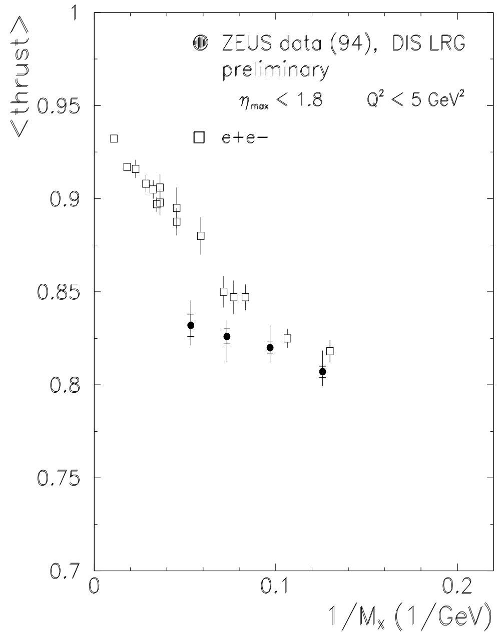

Figure 15: Correlation of thrust with $1/M_X$ from Zeus. The data are not corrected for the η_{max} cut.

with respect to the latter direction. Theoretical calculations of such correlations are becoming available [4]. The differential P_t^2 cross sections for six M_X intervals in the mass range from 6 to 36 GeV, normalized to the total cross sections in the respective M_X intervals, are shown in Fig. 16a. To exhibit the alignment features in a more visible way, the P_t^2 distribution of one mass range ($19 < M_X < 24$ GeV) is displayed in Fig. 16b on a linear scale in P_t^2. The data show

1. a steep rise of the distribution towards low P_t^2 values, demonstrating a dominant alignment of the final state thrust axis with the initial $\gamma^* p$ collision direction;

2. a shape of the P_t^2 distributions nearly independent of M_X, suggesting the factorizable form
$$\mathrm{d}\sigma(M_X, P_t^2)/\mathrm{d}P_t^2 = A(M_X) \cdot B(P_t^2);$$

3. a substantial large P_t^2 tail compatible with a P_t^{-4} dependence from 10 to 110 GeV^2.

The large high-P_t tail is further evidence for significant contributions from perturbative orders higher than $q\bar{q}$ [4], such as those shown in Figs. 10b-d.

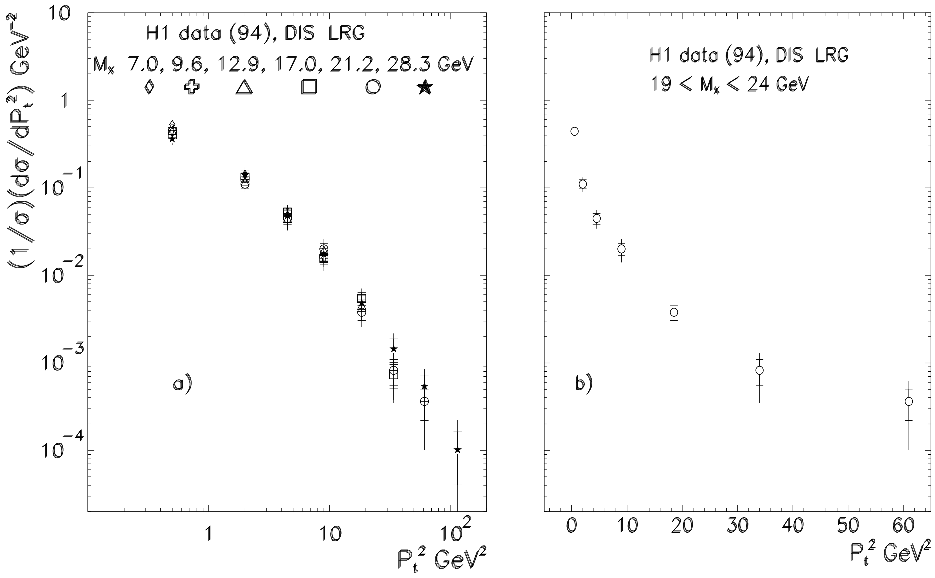

Figure 16a: Normalized thrust jet P_t^2 distributions for six M_X intervals. The P_t^2 bin limits are 0, 1, 3, 6, 12, 25, 43, 79, and 151 GeV^2; **16b:** Normalized thrust jet P_t^2 distribution for $19 < M_X < 24$ GeV, with a linear P_t^2 scale.

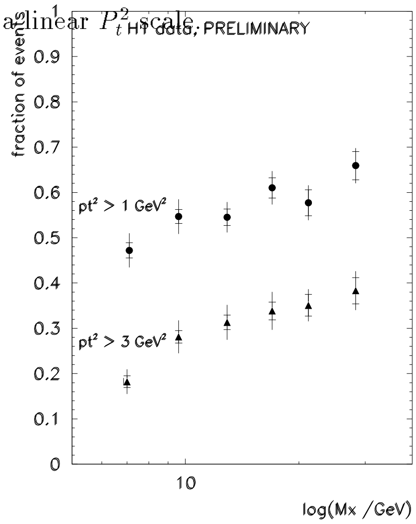

Figure 17: Event fractions with thrust jet $P_t > 1(3)$ GeV^2 as a function of M_X.

In Fig. 17 the fractions of events with P_t^2 values above 1.0 GeV^2 and above 3.0 GeV^2, respectively, are given as a function of M_X. The fraction at the lowest M_X point in Fig. 17 is relatively low because the kinematic range for $P_t^2 > 3$ GeV^2 is small here. For higher masses the fractions reach about 64% for $P_t^2 > 1$ GeV^2 and 35% for $P_t^2 > 3$ GeV^2. Such large values require that hard processes which involve more than two final state partons play an important role in the production mechanism of DIS LRG events.

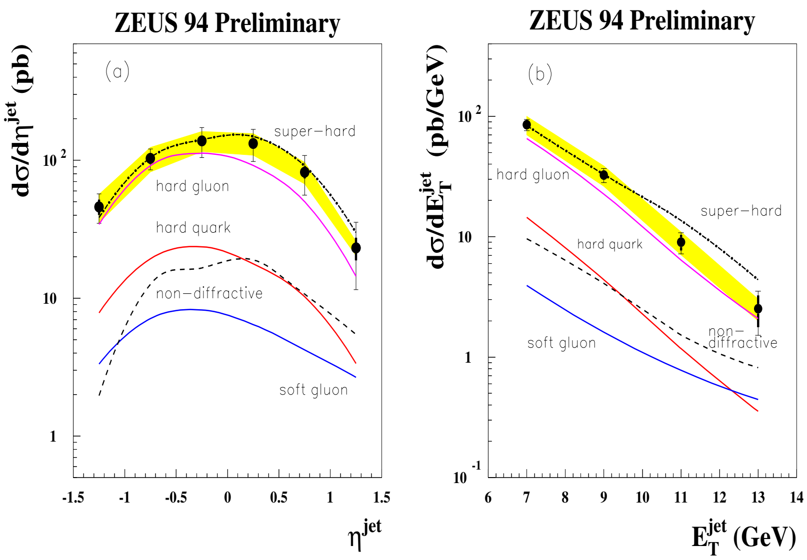

Figure 18: Photoproduction cross section for dijet production in LRG events, as a function of η^{jet} and E_T^{jet}. The curves are simulations with the POMPYT Monte Carlo program.

Similar partonic properties are also observed in diffractive photoproduction. A large and hard gluon density distribution like $\beta \cdot (1-\beta)$ in the POMPYT [21] Monte Carlo program is preferred to describe the dijet production in LRG photoproduction events in a ZEUS analysis. A soft gluon distribution $\propto (1-\beta)^5$ matches neither shape nor magnitude of the data, but normalization of pomeron flux and density distributions are quite uncertain. A hard quark density distribution is also compatible in the shapes.

6 Summary

1. HERA with its asymmetric e-p beams is an excellent laboratory to study the virtual hadron-parton states of real and virtual photons, by 'diffracting them into existence'.

2. We are still far from a precise factual picture, but we have learned:

- at low $Q^2(\lesssim 1 GeV^2)$
  quasi elastic diffraction (into VM's) and inelastic (into X $\neq$ VM) diffractive dissociation are of similar strength ($\simeq 10-15\%\ \sigma_{tot}$).
- at large $Q^2(\gg 1 GeV^2)$
  quasi elastic (=hadron-like) diffraction becomes negligible ($\sim 0.1\%\ \sigma_{tot}$)
  inelastic (= partonic ?) diffraction remains big ($\sim 10\%\ \sigma_{tot}$).

3. **Vector meson production $\gamma \rightarrow$ VM shows:**

- at low $Q^2 : \sigma(\gamma p \rightarrow \rho p) \simeq 200\sigma(\gamma p \rightarrow J/\psi p)$
  for $Q^2 > 10$ GeV^2 : $\sigma(\gamma^* p \rightarrow \rho p) \simeq 1\ \sigma(\gamma^* p \rightarrow J/\psi p)$, corresponding to the VM quark electric charges
- for large Q^2, and/or large M_V^2: the W dependence of $\sigma(\gamma p \rightarrow$ Vp) is much steeper than for hadron-hadron elastic scattering.
- e^{bt} and W^δ coeffients are correlated with the number of vertices having coherence at the hadron scale (N_{CHS}):
  $b\,(N_{CHS}) =\ 10\ (2),\ 5\ (1),\ 2\ (0)$ GeV^{-2}; $\quad \delta\,(N_{CHS}) =\ 0.22\ (2),\ 0.6\ (1),\ ?\ (0)$.

4. **Photon dissociation $\gamma^* \rightarrow$ X shows:**

- $\sigma(\gamma^* p \rightarrow pX; Q^2, W, M_X) \Longrightarrow \alpha_{I\!P}(0) \simeq 1.2$ only slightly harder than soft Regge behavior.
- parton structure of diffractive exchange:
  - gluon dominated (> 80 % of $I\!P$ momentum)
  - most of $I\!P$ momentum in one gluon.
- X = 2-jet like, strongly aligned with $\gamma^* p$ collision axis,
- thrust jets in LRG events are broader than in $e^+e^- \rightarrow \gamma^* \rightarrow$ hadrons.
  X $\neq q\bar{q}$ with limited p_t hadronization
  $q\bar{q}g$ configurations more important than in e^+e^-
- spins of X grow with M_X (consistent with $J_{max} \propto M_X$)
- large P_t tails of thrust jet momenta relative to $\gamma^* p$ collision axis demonstrate strong role of $q\bar{q}g$ processes.

7 Acknowledgements

I appreciate the informative discussions with M. Arneodo, A. Caldwell, J.P Fernandez, and R. Nania on ZEUS data, the support by many H1 colleagues, and the almost endless patience of M. Greco with me delivering this report.

References

[1] M.L. Good and W.D. Walker, Phys. Rev. 120 (1960) 1857.

[2] N.N. Nikolaev and B.G. Zakharov, Z. Phys. C49 (1991) 607;
S.J. Brodsky, P. Hoyer, and L. Magnea, "Rapidity gaps in perturbative QCD", preprint SLAC-PUB-7342, hep-ph/9611278;
S.J. Brodsky, A. Hebecker, and E. Quack, Phys. Rev. D55 (1997) 2584.

[3] W. Buchmüller and A. Hebecker, Phys. Lett. B355 (1995) 573.

[4] W. Buchmüller, M.F. McDermott, and A. Hebecker, "High-Pt Jets in Diffractive Electroproduction", preprint DESY 97-099, hep-ph/9706354.

[5] ZEUS Collab., M. Derrick et al., Phys. Lett. B315 (1993) 481.

[6] H1 Collab., T. Ahmed et al., Nucl. Phys. B429 (1994) 477.

[7] H1 Collab., T. Ahmed et al., Phys. Lett. B348 (1995) 681.

[8] ZEUS Collab., M. Derrick et al., Z. Phys. C68 (1995) 569.

[9] G. Ingelman and P.E. Schlein, Phys. Lett. B152 (1985) 256.

[10] Proceedings of the XXVIII International Conference on High Energy Physics, Warsaw, 1996.

[11] M.G. Ryskin, Z. Phys. C57 (1993) 89.

[12] J.D. Bjorken and J.B. Kogut, Phys. Rev. D8 (1973) 1341.

[13] A.B. Zamolodchikov, B.Z. Kopeliovich, and L.I. Lapidus, Pisma v. ZhETF 33 (1981) 612;
G. Bertsch et al., Phys. Rev. Lett 47 (1981) 267.

[14] L. Frankfurt and M. Strikman, Phys. Rep. 160 (1988) 235.

[15] S. Brandt et al., Phys. Lett. 12 (1964) 57.

[16] E. Farhi, Phys. Rev. Lett. 39 (1977) 1587.

[17] PLUTO Collab., Ch. Berger et al., Z. Phys. C12 (1982) 297.

[18] MARK II Collab., A. Peterson et al., Phys. Rev. D37 (1988) 1;
TASSO Collab., W. Braunschweig et al., Z. Phys. C45 (1989) 11 and Z. Phys. C47 (1990) 187.
AMY Collab., Y.K. Li et al., Phys. Rev. D41 (1990) 2675;
DELPHI Collab., P. Abreu et al., Z. Phys. C73 (1997) 229.

[19] R.D. Field and R.P. Feynman, Nucl. Phys. B136 (1978) 1.

[20] H. Jung, Comp. Phys. Comm. 86 (1995) 147.

[21] P. Bruni and G. Ingelman, "Monte Carlo program POMPYT", Proc. of the Intern. Europhysics Conference 1993, Marseille, France (Ed.Frontieres, Gif-sur-Yvette, 1994, p.595).